JACS
JOURNAL OF THE AMERICAN CHEMICAL SOCIETY
Article
pubs.acs.org/JACS

Efficient Energy Sensitization of C_{60} and Application to Organic Photovoltaics

Cong Trinh,[†] Kent O. Kirlikovali,[†] Andrew N. Bartynski,[‡] Christopher J. Tassone,[§] Michael F. Toney,[§] George F. Burkhard,[∥] Michael D. McGehee,[⊥] Peter I. Djurovich,[†] and Mark E. Thompson*[,†,‡]

[†]Department of Chemistry and [‡]Department of Chemical Engineering, University of Southern California, Los Angeles, California 90089, United States

[§]Materials Science Department, Stanford Synchrotron Radiation Lightsource, Menlo Park, California 94025, United States

[∥]Geballe Laboratory for Advanced Materials and [⊥]Department of Materials Science and Engineering, Stanford University, Stanford, California 94305, United States

Supporting Information

ABSTRACT: Fullerenes are currently the most popular electron-acceptor material used in organic photovoltaics (OPVs) due to their superior properties, such as good electron conductivity and efficient charge separation at the donor/acceptor interface. However, low absorptivity in the visible spectral region is a significant drawback of fullerenes. In this study, we have designed a zinc chlorodipyrrin derivative (ZCl) that absorbs strongly in the visible region (450−600 nm) with an optical density 7-fold higher than a C_{60} film. ZCl efficiently transfers absorbed photoenergy to C_{60} in mixed films. Application of ZCl as an energy sensitizer in OPV devices leads to an increase in the photocurrent from the acceptor layer, without changing the other device characteristics, i.e., open circuit voltage and fill factor. For example, C_{60}-based OPVs with and without the sensitizer give 4.03 and 3.05 mA/cm^2, respectively, while both have V_{OC} = 0.88 V and FF = 0.44. Our ZCl sensitization approach improves the absorbance of the electron-acceptor layer while still utilizing the beneficial characteristics of C_{60} in OPVs.

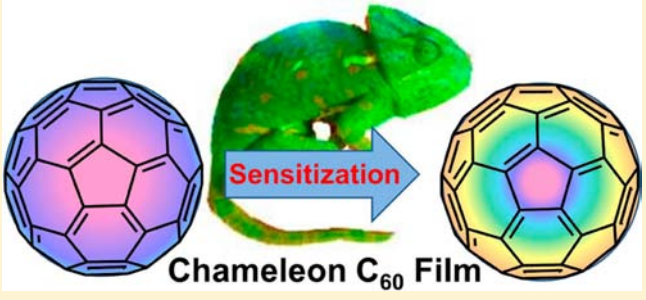

INTRODUCTION

Organic solar cells, or organic photovoltaics (OPV), are a promising energy source as they offer potential advantages over the conventional inorganic photovoltaics, including lightweight, flexibility, and low cost roll-to-roll production. A typical OPV device consists of separate electron-donor and -acceptor materials, which are responsible for light absorption and charge generation, as excitons dissociate at the donor/acceptor (D/A) interface.[1−3] While research has largely focused on the development of new donor materials, fullerenes remain the most popular acceptor materials because of their good electron conductivity[4−6] and ability to promote efficient D/A charge separation.[7,8] Fullerenes have been shown to perform well with a variety of donor materials,[8] and all of the reported high efficiency OPV devices utilize fullerene acceptors.[9] A key drawback of the most commonly used fullerene C_{60} is its low absorption in the visible part of the spectrum, due to the symmetry forbidden nature of the lowest energy electronic transition, λ = 670 nm. A neat C_{60} film shows a high optical density between 400−500 nm assigned to an intermolecular charge-transfer (CT) absorption.[10] The poor overlap of this C_{60} absorption with the AM1.5G solar flux (Figure 1) requires that the donor material(s) collect the majority of the incident photons. As absorption of the donor material is extended to the near-infrared (NIR), the green-to-orange part of the spectrum is left unabsorbed due to the relatively narrow absorption bands of organic dyes.[11−19]

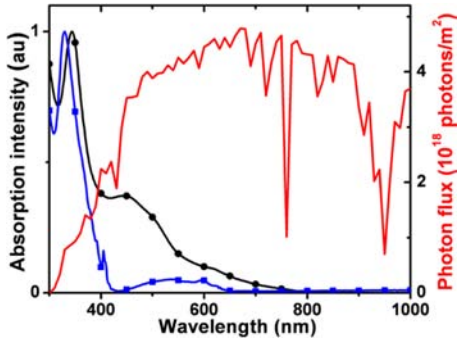

Figure 1. Absorption spectra of C60 in neat films (black circles), toluene solution (blue squares), and AM1.5G solar photon flux (red).

In order to efficiently harvest solar energy, it would thus be desirable to have new acceptor materials that strongly absorb visible light, while also retaining the favorable electron mobility

Received: May 10, 2013
Published: July 17, 2013

dx.doi.org/10.1021/ja4043356 | J. Am. Chem. Soc. 2013, 135, 11920−11928

and charge separation efficiencies found in fullerenes. In this way, light absorption could be more equitably distributed between the donor and acceptor materials, potentially allowing the device's photoresponse to be fully extended into the NIR. Unfortunately, the performance of nonfullerene acceptors is generally inferior to that of fullerenes.[7,8,20,21] Energy sensitization of fullerenes is an alternative method to improve both the breadth and the efficiency of visible light absorption in fullerene-based acceptors.

The sensitization of phenyl-C_{61}-butyric acid methyl ester (PCBM) using a perylene diimide (PDI) derivative has been recently reported by Hesse et al.[22] It was shown that the PCBM-PDI blend worked well with the UV-absorbing hexabenzocoronene donor but not with a red-NIR-absorbing polymer donor.[22] This dependence on donor material might be the result of dissimilarities between the molecular shapes of PDI (flat) and PCBM (ball-like), leading to unfavorable phase separation between the two acceptors. Moreover, while the singlet energy of PDI is higher than that of PCBM, the triplet energy of PDI (1.2 eV)[23,24] is lower (PCBM triplet = 1.55 eV). Thus, it is possible that singlet energy passed from PDI to PCBM can, after intersystem crossing (ISC), undergo triplet transfer back to PDI as was previously observed in a PDI-C_{60} dyad.[25−27] From the energetic standpoint, this energy ping-pong effect (illustrated in Figure 2a) is an undesirable process

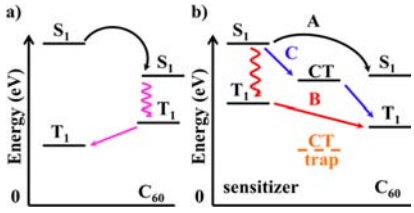

Figure 2. Energy diagram showing sensitization pathways in two cases: (a) a sensitizer (e.g., PDI or DCV3T) having higher singlet energy but lower triplet energy than C_{60} and (b) a sensitizer having both singlet and triplet energies higher than that of C_{60}. There are three possible pathways for sensitization: A, singlet transfer; B, triplet transfer; and C, electron transfer to form a CT state, which decay to triplet state of C_{60} if the CT state energy is higher than C_{60} triplet. If the energy of the CT state is lower than C_{60} triplet, it will act as a trap state (CT trap).

because the absorbed light energy is not confined to the fullerene, causing energy loss due to the low energy of sensitizer's triplet. In addition, even though a photoresponse from PDI was observed in a device using a blended PCBM-PDI acceptor layer, it remains unclear whether the observed photocurrent comes from energy sensitization of PCBM or from direct charge separation between PDI and the donor at the D/A interface. A similar energy ping-pong effect in a dicyanovinyl-terthiophene (DCV3T)-C_{60} acceptor blend has been intentionally utilized in OPV devices[28,29] where it was postulated that the triplet of DCV3T induced charge separation at the D/A interface.[29] Even though, as stated above, triplet transfer back to the sensitizer is undesired, in this case the conductivity and fill factor (FF) of OPV devices using these blended acceptors were improved compared to the devices using a neat DCV3T acceptor.

To take full advantage of the superior electron transport properties of C_{60} while minimizing possible energy loss by back triplet energy transfer from C_{60} to the sensitizer, the sensitized energy is confined to C_{60}. We have designed a blended acceptor layer where C_{60} is used as the host material that conducts both excitons and electrons and a sensitizer that serves as a light absorbing guest. Upon excitation of the sensitizer, energy is transferred to the C_{60} host and subsequently transported to the D/A interface where, after charge separation, electrons are conducted by the C_{60} host to the electrode. In our sensitization approach, metal dipyrrin complexes are employed to enhance the ability of a C_{60} based acceptor layer to generate photocurrent from absorption in the green-to-orange part of the solar spectrum. Energy sensitization to fullerenes has been previously explored in solution by studying covalently linked dyads containing fullerene and dipyrrins.[30,31] However, these compounds have not been used as sensitizers in solid state devices, such as OPVs, where the CT absorption band of C_{60} dominates the photoresponse.

RESULTS AND DISCUSSION

Molecular Design for Sensitizers. Three possible pathways to sensitize C_{60} via photoexcitation of a sensitizer are shown in Figure 2b: (A) singlet energy transfer, (B) triplet energy transfer, or (C) electron transfer from sensitizer to C_{60} followed by charge recombination to the triplet state of C_{60}. It is important that all three pathways be viable for the sensitization of C_{60}, because the nonviable pathway can act as an exciton or charge trap in the mixed C_{60} film. The three pathways impose several requirements for an efficient sensitizer: (1) Both singlet and triplet energies of the sensitizer need to be greater than C_{60} to guarantee efficient energy transfer to C_{60}. (2) the oxidation potential has to be sufficiently high to ensure that the energy of the CT state (i.e., $Sen^{-}C_{60}^{+}$), if formed, is greater than that of the triplet state of C_{60}, $E_{triplet}^{C60}$. To a first approximation, the CT energy is given by $-q(E_{ox}^{sen} - E_{red}^{C60}) - \Delta E_C$, where q is the elementary charge, E_{ox}^{sen} and E_{red}^{C60} are the oxidation potential of sensitizer and reduction potential of C_{60}, respectively, and ΔE_C (estimated ~0.3 eV)[32] is the Columbic interaction between the sensitizer cation and C_{60} anion. Given a C_{60} reduction potential of −1.06 V (vs Fc/Fc^{+}),[33] E_{ox}^{sen} must be >0.74 V to satisfy this criterion. If the energy of the CT state $Sen^{+}C_{60}^{-}$ is lower than C_{60} triplet state, it will serve as a net electron donor to C_{60},[34] forming a charge trap state in our host−guest acceptor layer (Figure 2b). This type of charge trapping is a potential problem in previous works that involved blending an additional donor material into C_{60} layer.[35,36] (3) In order to maintain good electron conductivity by the C_{60} host, the reduction potential of the sensitizer has to be lower (more negative) than C_{60} to ensure that electrons are conducted by C_{60} without being trapped by the sensitizer. (4) In addition, it is desirable that the molecular size and shape of the sensitizer should be similar to C_{60} so as to not severely disrupt the molecular packing and thus maintain good electron conductivity in the C_{60}-based acceptor layer. It should be emphasized that our design strategy is different from the previous works with PDI or DCV3T,[22,29] as all energy absorbed in the acceptor layer will ultimately be located on the C_{60} host.

Singlet and triplet energies as well as reduction and oxidation potentials of C_{60} are summarized in Table 1. While there are many organic dyes that have strong absorption in the visible spectrum and higher singlet energy than C_{60}, there are only a few classes of organic compounds exhibiting higher or similar triplet energy to C_{60} as well. Dipyrrins (E_T = 1.82 eV)[37] and porphyrins (1.60−1.65 eV)[38,39] meet these criteria, however the flat molecular shape of porphyrins is very different from C_{60}. Zinc dipyrrin complexes[40] have a quasi-spherical shape and size similar to C_{60}. Both singlet[40] and triplet[37] energies of

dx.doi.org/10.1021/ja4043356 | J. Am. Chem. Soc. 2013, 135, 11920−11928

Table 1. Photophysical and Electrochemical Properties of ZH, ZCl, and C_{60} in Solution and Thin Films

	solution						thin film	
	E_S (eV)[a]	E_T (eV)	E_{ox} (V)[b]	$E_{red}^{1/2}$ (V)[b]	QE (%)[f]	τ (ns)[f]	E_S (eV)[a]	E_T (eV)
ZH	2.54	1.82[c]	+0.71	−1.94	41	3.9	2.33	–
ZCl	2.37	1.75[c]	+1.22	−1.30	18	2.2	2.22	1.65
C_{60}	1.86	1.55[d]	+1.26[e]	−1.06	–	–	1.84	1.50, 1.44[d]

[a]Determined by the midpoint between the normalized absorption and emission spectra recorded in cyclohexane. [b]vs Fc^+/Fc. [c]Measured in 2-MeTHF at 77K. [d]Ref 45. [e]Ref 33. [f]In cyclohexane.

dipyrrin complexes are higher than those of C_{60}. Another benefit of the dipyrrin complexes over porphyrins is that the energy levels of zinc dipyrrins complexes are readily tunable via chemical modification of pyrrole rings or substituents at the meso position and prepared by straightforward synthetic procedures.[41] Zinc dipyrrins have been used as linkers and/or light absorbers in multichromorphoric light absorbing[40,42] or charge separating systems[43] in solution, but have not been used in OPV devices.

Synthesis and Characterization of the Sensitizer. The unsubstituted bis(5-mesityldipyrrinato) zinc (ZH) was synthesized and characterized following a published procedure.[42] Unfortunately, the oxidation potential of ZH (+0.71 V vs Fc^+/Fc) is not sufficient to satisfy requirement (2) above, and a low-energy CT state is expected, i.e., $ZH^+C_{60}^-$. Indeed, ZH can be used as a donor material in OPV devices using C_{60} as the acceptor (see SI). In order to raise the oxidation potential of zinc dipyrrin, high electron affinity substituents, i.e., Cl atoms, were added to the pyrrole rings.

The synthesis of a chlorinated zinc dipyrrin is summarized in Scheme 1. The final product was obtained as an inseparable mixture of two complexes, having either 11 (ZCl_{11}) or 12 (ZCl_{12}) chlorine atoms, in a respective molar ratio of 1:3 (17% yield). The unique site of the residual pyrrolic hydrogen of the ZCl_{11} derivative (indicated in red in Scheme 1) was confirmed by standard and 1D NOESY NMR techniques (SI). Attempts to separate these derivatives using column chromatography, recrystallization, or thermal gradient sublimation were unsuccessful. The ZCl_{12}:ZCl_{11} ratio could be increased using either longer reaction times or elevated temperatures; however, the yields obtained under these conditions were so unacceptably low (1−5%) that the 1:3 mixture of ZCl_{11}:ZCl_{12} (abbreviated ZCl) was used for all subsequent experiments. An X-ray analysis was performed on a co-crystal of ZCl_{11} and ZCl_{12}, and the molecular structure is shown in Figure 3 (the atom marked in red can be either H or Cl with an occupancy ratio H:Cl = 1:3). The two dipyrrin ligands are held nearly perpendicular to each other through Zn center with a dihedral angle of 87.6°, forming a quasi-spherical molecular shape. The

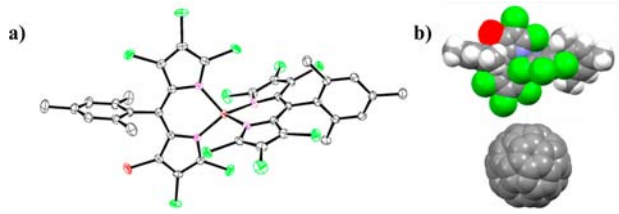

Figure 3. (a) ORTEP diagram of ZCl and (b) space filling models of ZCl (upper) and C_{60} (lower) with the proportional sizes as determined from X-ray single crystal data. The atom marked in red can be either H or Cl with an occupancy ratio H:Cl = 1:3.

molecular volume of ZCl (1000 Å^3) is similar to that of C_{60} (725 Å^3) as estimated from the crystal structure.[44]

Electrochemical measurements of ZCl carried out in dichloromethane with Fc^+/Fc as the internal standard are presented in Figure 4. ZCl undergoes irreversible oxidation at

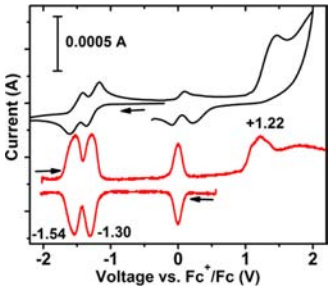

Figure 4. CV and DPV diagrams of ZCl in dichloromethane (vs Fc^+/Fc). Scan rate = 100 mV/s.

+1.22 V and two reversible reductions at −1.30 and −1.54 V (vs Fc^+/Fc). Since no discernible difference was observed in the redox potentials of ZCl_{11} and ZCl_{12}, the electronic properties of the two compounds were evaluated using DFT calculations. In agreement with the experimental data, ZCl_{11} and ZCl_{12} have similar energies for their respective highest occupied molecular orbitals (HOMO = −6.13 and −6.25 eV), lowest unoccupied molecular orbitals (LUMO = −3.23 and −3.29 eV), and triplet states (E_T = 1.70 eV for both).

The absorption and emission spectra of ZCl in cyclohexane solution and neat film are shown in Figure 5; the photophysical properties are summarized in Table 1. ZCl displays an intense absorption band between 450−600 nm and is strongly fluorescent in cyclohexane at room temperature (quantum yield = 18%, τ = 2.2 ns). Phosphorescence (λ_{max} = 710 nm, lifetime of ∼0.5 ms) of ZCl was observed in 2-methyltetrahydrofuran (2-MeTHF) at 77 K (Figure 4a). Chlorination slightly lowers both singlet and triplet states of ZCl compared to ZH by 170 and 70 meV, respectively. However, the singlet and triplet energies of ZCl are still significantly higher than C_{60}, satisfying requirement (1) for the sensitizer. Chlorination significantly

Scheme 1

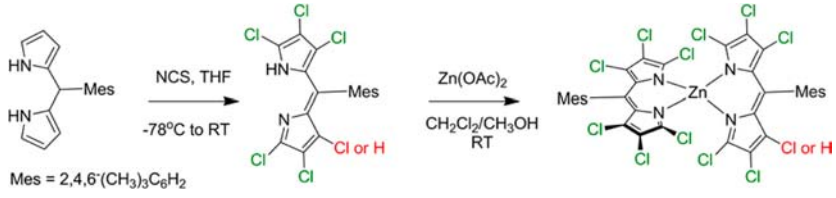

dx.doi.org/10.1021/ja4043356 | J. Am. Chem. Soc. 2013, 135, 11920−11928

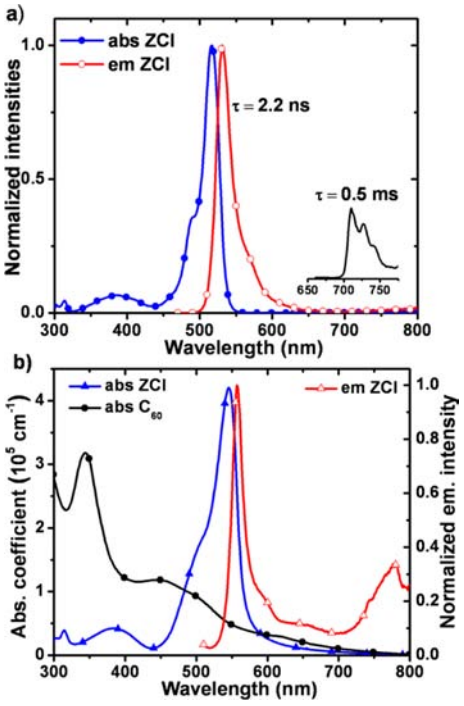

Figure 5. Absorption (blue) and emission (red) spectra of (a) solution of ZCl in cyclohexane at room temperature, inset is the phosphorescence of ZCl measured in 2-MeTHF at 77K, excitation = 460 nm and (b) ZCl film at room temperature, excitation = 460 nm. The thin film absorption spectrum of C_{60} is also shown for comparison.

increases the oxidation potential from +0.71 (ZH) to +1.22 V (ZCl). In addition, the reduction potential of ZCl is 240 mV more negative than that of C_{60}. Thus, the oxidation and reduction potentials of ZCl satisfy the sensitizer requirements (2) and (3), respectively.

The optical density of neat ZCl thin films is nearly 7-fold greater than that of C_{60} in the range between 470 and 570 nm (Figure 5b). Interestingly, both fluorescence and phosphorescence were observed in a neat film at room temperature (Figure 5b). Despite a 60 nm red shift of the phosphorescence peak of the thin film compared to that in 2-MeTHF solution at 77K, the triplet energy of ZCl is still 0.15 eV higher than that of C_{60}. Thus, the energy levels of ZCl in the neat films also fulfill the requirement (1) given above for the sensitizer. Moreover, significant overlap exists between ZCl emission and C_{60} absorption spectra, assisting singlet energy transfer from the sensitizer to the C_{60} host by the Förster mechanism.

Photosensitization Study. The photosensitization efficiency was quantified by Stern–Volmer quenching measurements of ZCl:C_{60} mixtures in toluene solution (see SI). ZCl emission is efficiently quenched by C_{60}, with a rate constant for luminescent quenching at the diffusion controlled limit. To examine whether energy transfer processes from ZCl to C_{60} will lead to sensitization in the solid state, absorption, and photoluminescence (PL) spectra were collected from neat C_{60} and mixed C_{60}:ZCl films with varied blending ratios (Figure 6). Note that the amount of C_{60} in these films is kept constant. In all blended samples, the fluorescence of ZCl was completely quenched, and emission bands with spectral profiles identical to neat C_{60} were observed between 700–900 nm. The luminescence from the thin films is assigned to the excited singlet state of C_{60} since the band shape and peak maximum

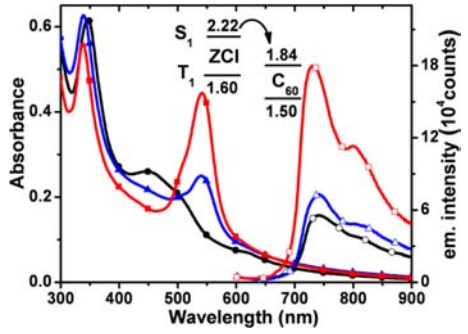

Figure 6. Absorption (solid symbols) and emission under excitation at 514 nm (open symbols) of 50 nm C_{60} film (black circle) and 59 nm C_{60}:ZCl film (blue triangle, 15% ZCl by volume) and 75 nm C_{60}:ZCl film (red square, 35% ZCl by volume). Also shown is an energy level diagram (eV) for energy transfer from ZCl to C_{60}.

(λ_{max} = 737 nm) match well with published fluorescence spectra of C_{60}[46,47] and differ markedly in peak position from the phosphorescence of ZCl (Figure 5). The fluorescence intensity increased with higher ZCl content and consequent rise in absorbance from the blended films. Thus, the PL measurements indicate that photoexcited ZCl transfers energy to the C_{60} host in the thin films, resulting in increased fluorescence from C_{60}. The luminescent quenching of ZCl could occur via either Förster energy transfer or through an electron transfer mechanism to form a $ZCl^+C_{60}^-$ CT intermediate. The energy of this CT state is estimated to be 2.0 eV, so it would be expected to transfer energy to C_{60}, promoting it to its singlet excited state.[31,34]

Another sensitization pathway in the C_{60}:ZCl blend is triplet energy transfer from ZCl to C_{60} (pathway B in Figure 2b). Luminescent spectra of ZCl in both solution and neat solid clearly show competitive ISC to the triplet state. However, the rate of ISC is at best 3.7×10^8 s^{-1}, which is orders of magnitude smaller than the quenching rate constant by C_{60} determined from Stern–Volmer quenching experiments. Regardless, any triplets formed on ZCl can be subsequently transferred to the lower triplet state of C_{60}. Thus, in all possible pathways of either singlet, triplet, or electron transfers from the ZCl to the C_{60}, the triplet energy of C_{60} is the lowest state, assuring that the sensitized energy is cascaded to the C_{60} host according to the design presented in Figure 2b.

Morphology of C_{60}:ZCl Films. Since the blended C_{60}:ZCl films will be used in OPV devices, it is important to understand any effect that the presence of ZCl has on molecular packing of C_{60} in the solid state or phase separation of the mixture. Atomic force microscopy (AFM) and grazing incident X-ray diffraction (GIXD) measurements were carried out on thin films of C_{60} (50 nm), ZCl (50 nm), and mixed C_{60}:ZCl (1:1, 100 nm), and the results are presented in Figure 7. GIXDs of neat ZCl films and mixed C_{60}:ZCl films at different concentrations are presented in SI. The neat C_{60} film shows six diffraction peaks at 0.77, 1.27, 1.48, 2.01, 2.19, and 2.32 $Å^{-1}$, which are indexed to the fcc crystal phase as the 111, 220, 311, 420, 422, and 333 peaks, respectively,[48] whereas the neat films of ZCl are amorphous. Upon addition of ZCl, the C_{60} phase becomes substantially more disordered as indicated by the dramatic broadening of the diffraction rings, reduced peak intensity, and the inability to resolve the 220 and 311 peaks. Thus, the GIXD measurements show that the mixed films become nanocrystalline or amorphous upon addition of the ZCl sensitizer.

dx.doi.org/10.1021/ja4043356 | J. Am. Chem. Soc. 2013, 135, 11920–11928

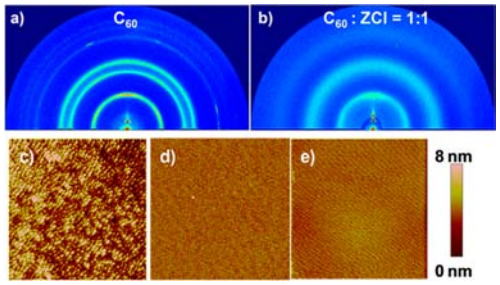

Figure 7. GIXD data of (a) neat C_{60} and (b) mixed C_{60}:ZCl 1:1 films on Si substrates. AFM images (5 × 5 μm) of (c) neat C_{60}, (d) mixed C_{60}:ZCl 1:1 by volume and (e) neat ZCl films on Si substrates.

Analysis by AFM techniques also supports a decrease in molecular order in the blended ZCl:C_{60} films. AFM images of neat films of C_{60} were found to be rough (rms = 1.85 nm), whereas neat films of ZCl were smooth (rms = 0.59 nm). Interestingly, the AFM image of the 1:1 mixed film shows no sign of phase separation and is quite smooth (rms = 0.39 nm). The phase sensitive AFM image showed no features, consistent with homogeneously mixed film. Thus, the AFM and GIXD data indicate that ZCl guest molecules are homogeneously dispersed in the C_{60} host, which is likely due to similar the sizes and shapes of both compounds. Homogeneous dispersion of ZCl into C_{60} is also beneficial for efficient photosensitization as the ZCl molecules will be located in close proximity to the C_{60} molecules.

Application in OPV Devices. OPVs were fabricated with a common multilayer structure of ITO/MoO_3/donor/acceptor/buffer/Al. Since the purpose of this work is to explore the sensitization process in the visible spectrum, the UV absorbing *N*,*N*′-di-[(1-naphthyl)-*N*,*N*′-diphenyl]-1,1′-biphenyl)-4,4′-diamine (NPD) was chosen as the donor material. NPD shows negligible absorption at wavelengths longer than 400 nm, which allows the photoresponse from the ZCl sensitizer and C_{60} to be unambiguously assigned. MoO_3 is used to improve hole extraction efficiency from the donor layer. The acceptor layer can be neat C_{60} or mixed C_{60}:ZCl with various architectures, and the buffer layer is bathocuproine (BCP). In the reference device, the optimal thickness of the neat C_{60} acceptor layer is 40 nm, increasing C_{60} thickness results in the decrease in photocurrent and subsequently lower device efficiency (see Table S1). Thus, the thickness of C_{60} used in reference devices is kept constant at 40 nm.

There are several ways to construct the sensitized devices; one straightforward method is to deposit the mixed C_{60}:sensitizer film with varied sensitizer concentrations directly on the donor layer, as was done in previous works.[22,29] Unfortunately, this simple architecture creates ambiguity as to whether any photoresponse from the sensitizer originates from photosensitization of C_{60} or from direct charge separation between donor and sensitizer at the D/A interface. Thus, sensitized devices with a structure ITO/MoO_3/NPD/C_{60}/C_{60}:ZCl/BCP/Al were constructed to prevent any direct contact of ZCl with the donor layer. Current−voltage (*J*−*V*) and external quantum efficiency (EQE) curves of OPV devices utilizing a C_{60}:ZCl layer with 15% (D2) and 50% (D3) of ZCl by volume on top of a thin C_{60} layer (5 nm) are presented in Figure 8. The device characteristics are summarized in Table 2. The values for the open circuit voltage (V_{OC}) and fill factor (FF) in both sensitized devices remain unchanged from those for the reference device D1. Seeing as all three devices have the

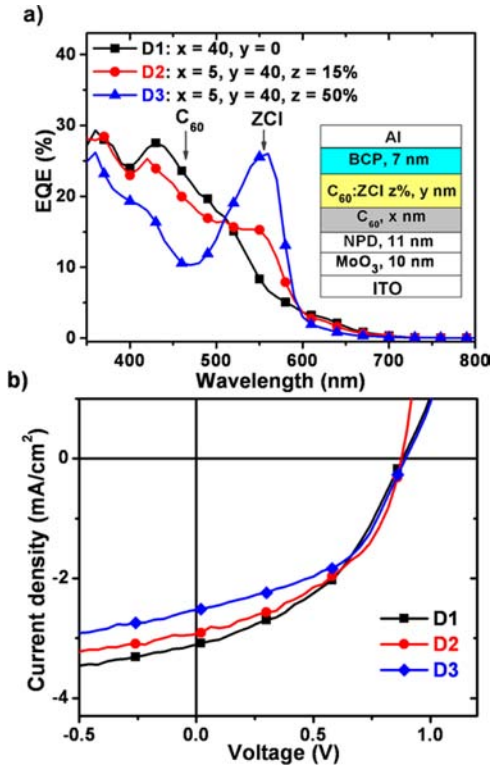

Figure 8. Structure and characteristics of OPV devices using an NPD donor layer with and without ZCl. (a) Plot of EQE, inset is the device structure, and (b) *J*−*V* curves of devices under 1 sun AM1.5G illumination.

same NPD/C_{60} interface, the thermodynamics and kinetics of the charge separation/recombination processes at this DA boundary are identical, and consequently, the V_{OC} is unaffected. The unaltered FF value in devices D2−3 indicates that the charge collection efficiency is well maintained despite the lower crystallinity of the mixed C_{60}:ZCl film. The high conductivity of C_{60}, along with the similar size and shape of ZCl and C_{60}, allows a homogeneous C_{60}:ZCl layer to form with sufficient percolation pathways in C_{60} to enable good electron conduction. In a related study, we have investigated the effect of mixing an inert material, BCP, into C_{60} and found that the conductivity of C_{60} was not affected even in films that had up to 50% BCP by volume, i.e., the same ZCl loading used here.[49]

The photocurrents of the devices drop as the ZCl concentration increases, D1 > D2 > D3. The reduction in photocurrent can be understood from EQE measurements (Figure 8a). EQE clearly indicates the contribution of the sensitizer ZCl (peak maximum at 550 nm) to the photocurrents in devices D2 and D3, with the ZCl photoresponse proportional to its concentration. As there is no direct contact between ZCl and the donor layer, the increased photoresponse between 500 and 600 nm in D2 and D3 must come from photoenergy absorbed by ZCl and subsequently transferred to C_{60}. In contrast, the photoresponse from C_{60} decreases as ZCl concentration increases in devices D2 and D3. The loss of C_{60} response is due to the decrease in absorption of C_{60} as blending concentration increases.[49] This decrease is slightly larger than the increase due to ZCl sensitization, resulting in a net decrease in the photocurrent of D2 and D3.

It is desirable to maintain the photoresponse from C_{60} while maximizing the photoresponse from the sensitizer ZCl, thus

dx.doi.org/10.1021/ja4043356 | J. Am. Chem. Soc. 2013, 135, 11920−11928

Table 2. Characteristics of OPV Devices under Spectral Mismatch Factor Corrected 1 sun AM1.5G Illumination[a]

device	structure of the acceptor layers	J_{SC} (±0.05 mA/cm^2)	V_{OC} (±0.01 V)	FF (±0.01)	η (±0.04%)
		Donor = NPD, 11 nm			
D1	C_{60}, 40 nm	3.04	0.88	0.44	1.19
D2	C_{60}, 5 nm/C_{60}:ZCl (5.6:1), 40 nm	2.92	0.89	0.46	1.17
D3	C_{60}, 5 nm/C_{60}:ZCl (1:1), 40 nm	2.51	0.88	0.46	1.06
D4	C_{60}, 15 nm/C_{60}:ZCl (1:1), 30 nm	3.87	0.89	0.43	1.48
D5	C_{60}, 25 nm/C_{60}:ZCl (1:1), 20 nm	3.53	0.89	0.44	1.35
D6	C_{60}, 35 nm/C_{60}:ZCl (1:1), 10 nm	3.23	0.88	0.44	1.25
D7	C_{60}, 15 nm/C_{60}:ZCl (1:1), 50 nm	4.03	0.88	0.44	1.56
D8	C_{60}, 25 nm/C_{60}:ZCl (1:1), 50 nm	3.90	0.90	0.44	1.48
		Donor = SQ, 11 nm			
D9	C_{60}, 40 nm	5.88	0.76	0.53	2.39
D10	C_{60}, 15 nm/C_{60}:ZCl (1:1), 50 nm	7.07	0.78	0.51	2.78

[a]Common device structure: ITO/MoO_3 (10 nm)/D/A/BCP (7 nm)/Al.

sensitized devices with a high ZCl concentration (50%) were chosen for further optimization. In order to determine the thickness of neat C_{60} needed to recover the its photoresponse, a series of devices consisting of a constant thickness of the acceptor layer (45 nm) and varied thicknesses of the neat C_{60} layer at D/A interface, ITO/MoO_3/NPD/C_{60} (x nm)/C_{60}:ZCl (1:1, 45 − x nm)/BCP/Al, has been fabricated. EQE measurements of these devices are presented in Figure 9, and

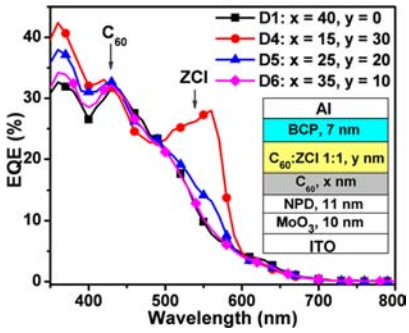

Figure 9. EQE measurements of sensitized devices with varied C_{60} layer thicknesses at the D/A interface.

the device characteristics are summarized in Table 2. As the thickness of the neat layer of C_{60} increases from 5 nm (D3) to 15 nm (D4), the photoresponse of C_{60} is fully recovered, while a significant contribution from ZCl is still observed. A further increase of C_{60} thickness to 25 nm (D5) markedly decreases the ZCl photoresponse along with the same response photoresponse from C_{60}. When 35 nm of C_{60} is used (D6), no photoresponse from ZCl is observed despite much higher optical density of ZCl compared to C_{60} (Figure 5b), likely due to limited diffusion length of the sensitized excitons.

Sensitized devices with a 15 nm of C_{60} at the D/A interface, the minimal thickness necessary for C_{60} photoresponse recovery, were further optimized by varying the thicknesses of the mixed C_{60}:ZCl (1:1) layer. The results are presented in Figure 10a. Similar to other sensitized devices, the FF and V_{OC} remains largely unchanged, and only photocurrent J_{SC} varies as the thickness of mixed C_{60}:ZCl layer changes. The J_{SC} value maximizes at a mixed layer thickness of 50 nm. Compared to the control device D1 using only neat C_{60} as acceptor layer, D7 exhibits a markedly higher photocurrent (ΔJ_{SC} = 1.0 mA/cm^2). Thus, the improved J_{SC}, in combination with unchanged V_{OC} and FF, results in an increase of the power conversion efficiency

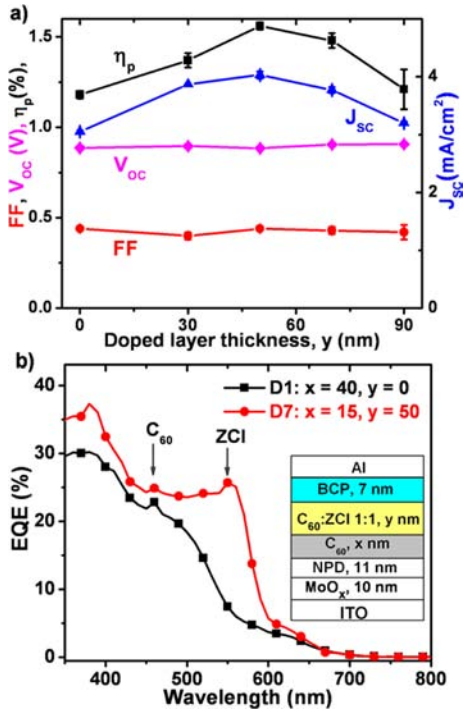

Figure 10. (a) Characteristics of sensitized devices with a neat layer of C_{60} (x = 15 nm) and varied thicknesses (y nm) of the blended C_{60}:ZCl layers; y = 0 represents the reference device with 40 nm of neat C_{60} as the acceptor layer; and (b) plot of EQE of D1 and optimized device using sensitizer (D7), inset is the device structure.

from 1.16% (D1) to 1.56% (D7). Further increasing the thickness of neat C_{60} at the D/A interface from 15 nm (D7) to 25 nm (D8) results in slight decrease in photocurrent and subsequent efficiency (Table 2). Thus, the acceptor layer used in D7 is the optimal structure for the sensitized devices.

As the absorption of donor materials is extended to the red-NIR part of spectrum, the green-to-orange part is left unabsorbed; 2,4-bis[4-(*N*,*N*-diisobutylamino)-2,6-dihydroxyphenyl] squaraine (SQ)[50] and zinc phthalocyanine (ZnPc) donor-based OPVs illustrate this problem (Figure 11 and SI). There are minima in the EQE curves at roughly 550 nm in both SQ/C_{60} and ZnPc/C_{60} devices where neither donor (ZnPc or SQ) nor C_{60} absorb effectively. The absorption of ZCl matches well with the EQE minima, thus ZCl can potentially be used to fill up the absorption gap in SQ and ZnPc OPV devices.

dx.doi.org/10.1021/ja4043356 | J. Am. Chem. Soc. 2013, 135, 11920−11928

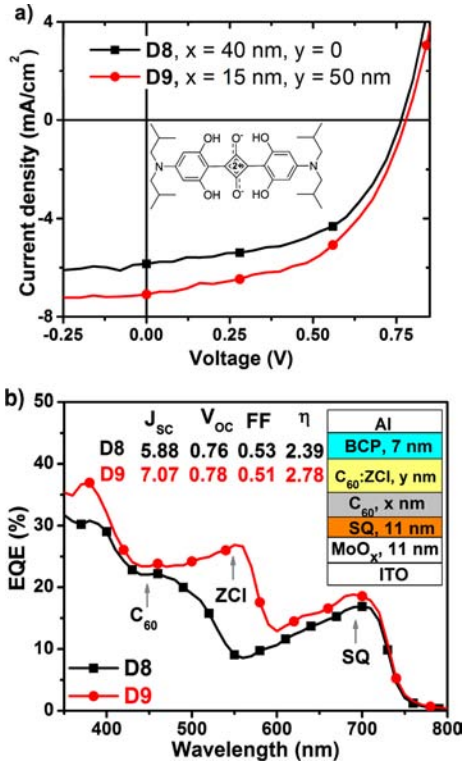

Figure 11. Structure and characteristics of OPV devices using a SQ donor layer with and without a sensitizer. (a) *J*–*V* curves of devices under 1 sun AM1.5G illumination, inset is the SQ structure (b) plot of EQE.

Sensitized devices with the optimal acceptor structure have been fabricated with ZnPc and SQ. As indicated by EQE measurements (Figure 11), the photoresponses from SQ and C_{60} remain unchanged, while the ZCl response nicely fills up the dip in the EQE curve, leading to a photocurrent improvement of 1.0–1.2 mA/cm^2 without any other change in the device characteristics. This increase of photocurrent is comparable to what was observed in the NPD/C_{60} device (Figure 10). Similar improvement is observed when ZCl is used in ZnPc/C_{60} OPV devices (see SI). Thus, the obtained results demonstrate that the ZCl sensitizer can be used with a variety of donor materials.

■ CONCLUSION

In summary, we have shown a set of energetic requirements and molecular design for a C_{60} sensitizer. An ideal sensitizer should have higher singlet and triplet energies than C_{60} and sufficiently high oxidation energy to give a $Sen^+C_{60}^-$ CT state a higher energy than the C_{60} triplet exciton. A chlorinated zinc dipyrrin ZCl, which satisfies all requirements for the sensitizer, was synthesized and fully characterized. Stern–Volmer quenching experiment and PL measurements of mixed C_{60}:ZCl films show that ZCl efficiently transfers absorbed photoenergy to C_{60}.

The OPV devices employing the C_{60}:ZCl host–guest acceptor layer have been constructed and optimized to demonstrate the sensitization approach. The optimal acceptor layer consisting of a neat C_{60} (15 nm) and a mixed C_{60}:ZCl (1:1, 50 nm) films has been used to maintain the beneficial properties of C_{60} while taking advantages of ZCl absorption. In the sensitized devices with various donor materials, efficient energy transfer from the photoexcited state of ZCl to C_{60} can increase the photoresponse of the acceptor layer up to 33% without changing other device characteristics. The sensitization approach presented here could potentially be used for multiple sensitizers to extend the absorption range of the electron-acceptor layer. While we have focused on the C_{60} acceptor layer in the present study, a similar approach could be used with other fullerenes as well as sensitized donor layers to broaden the photoresponse of OPVs.

■ EXPERIMENTAL SECTION

Instrumentation. GIXD measurements were performed at the Stanford Synchrotron Radiation Lightsource (SSRL) on beamline 11-3 with a photon wavelength of 0.0974 nm. The diffraction intensity was detected on a 2D image plate (MAR 345) with a pixel size of 150 μm (2300 × 2300 pixels). GIXD images were analyzed using the software package WxDiff, provided by Dr. Stefan Mannsfeld. The samples were 20 mm long in the direction of the beam path, and the detector was located 398.8 mm from the sample center. The beam incidence angle was 0.12°, and the beam size was 50 × 150 μm. The data presented here were corrected for the grazing incidence geometry. NMR measurements were performed on a Varian Mercury 500 MHz spectrometer. AFM was performed using a Digital Instruments Nanoscope Dimension 3100 atomic force microscope. UV–vis spectra were recorded on a Hewlett-Packard 4853 diode array spectrometer. Fluorescence lifetime measurements were performed by a time-correlated single-photon counting method using an IBH fluorocube lifetime instrument by equipped with a 405 nm LED excitation source. Quantum efficiency measurements were carried out using a Hamamatsu C9920 system equipped with a xenon lamp, calibrated integrating sphere and model C10027 photonic multichannel analyzer. CV and DPV measurements were performed using an EG&G Potentiostat/Galvanostat model 283. Dry dichloromethane from VWR was used as solvent under a N_2 atmosphere with 0.1 M tetra(*n*-butyl)ammonium hexafluorophosphate (Aldrich) as the supporting electrolyte. A glassy carbon working electrode and a platinum counter electrode were used, with a silver wire as the pseudoreference electrodes. The oxidation potential was measured relative to a ferrocenium/ferrocene (Fc^+/Fc) redox couple as an internal standard.

PL of ZCl in Solution and Thin Film. Steady-state emission measurements of ZCl in the thin film and solutions at room temperature and 77 K were performed using a Photon Technology International QuantaMaster Model C-60SE spectrofluorimeter.

PL measurements of C_{60} and C_{60}:ZCl Films. No emission was detected from neat C_{60} and mixed C_{60}:ZCl films using the Photon Technology International QuantaMaster Model C-60SE spectro-fluorimeter. The samples under nitrogen atmosphere were excited by 514 nm emission lines from a Spectra-Physics Stability 2017 argon ion laser. PL was measured by imaging the excited area of the sample onto the entrance slit of an Acton Research Spectrapro 500i spectrograph coupled to a cooled Hamamatsu CCD detector. The acquired data were corrected for the responses of the CCD array and the diffraction grating.

X-ray Data and Collection for ZCl. A metallic intense pink-green rhombic-like specimen of $C_{36}H_{22.25}Cl_{11.75}N_4Zn$, approximate dimensions 0.26 × 0.29 × 0.38 mm, was used for the X-ray crystallographic analysis. The X-ray intensity data were measured on a Bruker APEX II CCD system equipped with a TRIUMPH curved-crystal monochromator and a MoKα fine-focus tube (λ = 0.71073 Å).

A total of 2520 frames were collected. The total exposure time was 3.50 h. The frames were integrated with the Bruker SAINT software package using a SAINT V7.68A algorithm. The integration of the data using a monoclinic unit cell yielded a total of 96 239 reflections to a maximum θ angle of 30.56° (0.70 Å resolution), of which 12 079 were independent (average redundancy 7.967, completeness = 98.3%, R_{int} = 3.01%, R_{sig} = 1.81%) and 10 440 (86.43%) were >2σ (F^2). The final cell constants of *a* = 8.4166(4) Å, *b* = 23.9579(10) Å, *c* = 20.3078(9)

dx.doi.org/10.1021/ja4043356 | J. Am. Chem. Soc. 2013, 135, 11920–11928

Å, β = 101.4330(10)°, volume = 4013.7(3) Å^3, are based upon the refinement of the XYZ-centroids of 9012 reflections above 20 $\sigma(I)$ with 4.431° < 2θ < 60.92°. Data were corrected for absorption effects using the multiscan method (SADABS). The ratio of minimum to maximum apparent transmission was 0.901. The calculated minimum and maximum transmission coefficients (based on crystal size) are 0.6150 and 0.7086.

The structure was solved and refined using the Bruker SHELXTL software package, using the space group $P12_1/c1$, with Z = 4 for the formula unit, $C_{36}H_{22.25}Cl_{11.75}N_4Zn$. The final anisotropic full-matrix least-squares refinement on F^2 with 485 variables converged at $R1$ = 2.78%, for the observed data and w$R2$ = 6.65% for all data. The goodness-of-fit was 1.031. The largest peak in the final difference electron density synthesis was 0.945 e$^-$/Å^3, and the largest hole was −0.619 e$^-$/Å^3 with an rmsd of 0.060 e$^-$/Å^3. On the basis of the final model, the calculated density was 1.643 g/cm^3 and F(000), 1984 e$^-$.

Computational Methods. All calculations were performed using Titan software package (Wave function Inc.). The gas-phase geometry optimization was calculated using B3LYP functional with the LACVP** basis set as implemented in Titan. The energy levels and orbital diagrams of the HOMO and LUMO were obtained from the optimized geometry of the singlet state. The energy of the triplet state was calculated from the optimized triplet geometry.

Synthesis of ZCl. Synthesis of 5-mesityldipyrromethane (DPM) was performed following a published procedure.[51] A solution of DPM (0.62 g, 2.34 mmol) in 60 mL freshly distilled tetrahydrofuran (THF) was prepared; the solution was cooled down using dry ice/acetone bath and was bubbled with nitrogen for 5 min. A solution of *N*-chlorosuccinimide (3.1 g, 23.4 mmol) in 70 mL THF was prepared and slowly added to the DPM solution under nitrogen. The reaction mixture was stirred and allowed to warm up to room temperature during 2 h. The reaction mixture turned a dark-red color. After stirring for additional 2 h at room temperature, the reaction was stopped. The solvent was removed under reduced pressure, and the crude products were dissolved in 300 mL dichloromethane. The crude products were washed with $NaHCO_3$ solution twice and brine twice. The dark-red solution of the products in dichloromethane was used without further purification.

A solution of $Zn(OAc)_2{\cdot}2H_2O$ (2.5 g) in 30 mL CH_3OH was prepared and added to the solution of the dark-red products. The reaction turned into dark-green color and emitted a green-yellow color under UV lamp illumination. The reaction mixture was stirred overnight. The solvents were removed under reduced pressure. The solid reaction mixture was dissolved in dichloromethane, and inorganic salts were filtered off. The solution was washed with Na_2CO_3 solution twice and brine once. The solvent was removed. The crude product was passed through short neutral Al_2O_3 flash column using dichloromethane/hexanes (1/9) as eluent, and the orange-red fraction was collected. After removing the solvents, a dark-red product was collected. The product was dissolved in DCM and recrystallized by layering MeOH on top. Red-green crystals (ZCl) were collected (0.2 g, 17% total yield). ZCl was further purified by gradient sublimation under vacuum (10^{-5} Torr) at 280, 200, and 140 °C gradient temperature zones. The sublimed crystals were qualified for X-ray single crystal structure determination.

The product ZCl is a mixture of two compounds $C_{36}H_{22}Cl_{12}N_4Zn$ and $C_{36}H_{23}Cl_{11}N_4Zn$ with a molar ratio of 3:1 (general formula: $C_{144}H_{89}Cl_{47}N_{16}Zn_4$). ^{1}H NMR (400 MHz, $CDCl_3$): δ ppm 6.95 (s, 4H, mesityl), 6.49 (s, 0.23 H, pyrrole), 2.40−2.35 (m, 6H, mesityl), 2.09−2.04 (m, 12H, mesityl). ^{13}C NMR (500 MHz, $CDCl_3$): δ (ppm) 147.00, 143.29, 139.29, 136.04, 135.55, 132.46, 132.33, 130.30, 130.26, 129.74, 129.13, 128.43, 119.36, 118.70, 21.34, 21.23, 19.49, 19.42. HRMS: $C_{36}H_{22}Cl_{12}N_4Zn$: calcd, 999.7304; found, 999.7333. $C_{36}H_{22}Cl_{11}N_4Zn$: calcd, 965.7694; found, 965.7705. Elemental analysis: theoretical C, 43.55%; H, 2.26%; N, 5.64%. Found: C, 43.54%; H, 1.96%; N, 5.50%.

Device Fabrication and Characterization. Glass substrates coated with patterned ITO (width of patterned stripes is 2 mm, thickness = 150 ± 10 nm; sheet resistance = 20 ± 5 Ω cm^{-2}; transmission 84% at 550 nm; courtesy of Thin Film Devices, Inc.) were cleaned with soap and boiled in tetrachloroethylene, acetone, and propanol (5 min each). ITO substrates were exposed to ozone atmosphere (UVOCS T10 × 10/OES) for 10 min immediately before loading into the high-vacuum chamber. Deposition rates for layers of neat materials: MoO_x (0.05 nm/s), NPD (0.15 nm/s), SQ (0.1 nm/s), ZnPc (0.2 nm/s), C_{60} (0.2 nm/s), BCP (0.15 nm/s), and Al (0.2 nm/s). Deposition rates for mixed films (% ZCl content by volume): C_{60}:ZCl (15% ZCl) − codeposition C_{60} (0.2 nm/s):ZCl (0.035 nm/s); C_{60}:ZCl (35% ZCl) − codeposition C_{60} (0.1 nm/s):ZCl (0.05 nm/s); and C_{60}:ZCl (50% ZCl) − codeposition C_{60} (0.05 nm/s):ZCl (0.05 nm/s). After organic depositions, masks with 2 mm stripe width were placed on substrates under N_2, and 100 nm of Al electrode was deposited. Area of devices is 4 mm^2. Current−density dependence on applied test voltage $J(V)$ measurements were performed in air at 25 °C using a Keithley 2420 Sourcemeter (sensitivity = 100 pA) in the dark and under ASTM G173-03 spectral mismatch corrected 1000 W/m^2 white light illumination from an AM1.5G filtered 300 W xenon arc lamp (Newport Oriel). Routine spectral mismatch correction was performed using a silicon photodiode (Hamamatsu S1787−04,8RA filter) calibrated at the National Renewable Energy Laboratory (NREL). Chopped and filtered monochromatic light (250 Hz, 10 nm fwhm) from a Cornerstone 260 1/4 M double grating monochromator (Newport 74125) was used in conjunction with an EG&G 7220 lock-in amplifier to perform all spectral responsivity and spectral mismatch correction measurements.

■ ASSOCIATED CONTENT

Supporting Information

A detailed attribution for contributions from funding agencies; electrochemical measurements of ZH; ^{1}H, ^{13}C and NOESY ^{1}H NMR of ZCl; emission of ZCl in 2-MeTHF at 77 K; calculated energy levels and MOs of ZCl_{11} and ZCl_{12}; details of the Stern−Volmer quenching experiment; GIXD of mixed C_{60}:ZCl films at various concentrations; characteristics of sensitized devices with various C_{60}:ZCl (1:1) layer thicknesses; characteristics of devices using ZnPc and ZH donor layers; crystal data of ZCl. This material is available free of charge via the Internet at http://pubs.acs.org.

■ AUTHOR INFORMATION

Corresponding Author

met@usc.edu

Notes

The authors declare the following competing financial interest(s): One of the authors (M.E.T.) has a financial interest in the Global Photonic Energy Corporation.

■ ACKNOWLEDGMENTS

Financial support from Global Photonic Energy Corporation (GPEC), Department of Energy (DOE), Center for Energy Nanoscience (CEN) at USC, National Science Foundation (NSF) and King Abdullah University of Science and Technology (KAUST), through the Center for Molecular Photovoltaics (CAMP) is gratefully acknowledged. Details of how each funding agency supported this work are given in the Supporting Information. We thank Dr. Ralf Haiges for the help in refining single crystal structure, Dr. Travis Williams for the help in NOESY ^{1}H NMR experiment, and Drs. Sarah Conron and Zhiwei Liu for helpful discussions.

■ REFERENCES

(1) Clarke, T. M.; Durrant, J. R. *Chem. Rev.* **2010**, *110*, 6736−6767.
(2) Hains, A. W.; Liang, Z.; Woodhouse, M. A.; Gregg, B. A. *Chem. Rev.* **2010**, *110*, 6689−6735.

(3) Schlenker, C. W.; Thompson, M. E. *Chem. Commun.* **2011**, *47*, 3702−3716.
(4) Anthopoulos, T. D.; Singh, B.; Marjanovic, N.; Sariciftci, N. S.; Ramil, A. M.; Sitter, H.; Colle, M.; de Leeuw, D. M. *Appl. Phys. Lett.* **2006**, *89*, 213504.
(5) Zhang, X. H.; Kippelen, B. *Appl. Phys. Lett.* **2008**, *93*, 133305.
(6) Zhang, X.-H.; Kippelen, B. *J. Appl. Phys.* **2008**, *104*, 104504.
(7) Lin, Y.; Li, Y.; Zhan, X. *Chem. Soc. Rev.* **2012**, *41*, 4245−4272.
(8) Mishra, A.; Baeuerle, P. *Angew. Chem., Int. Ed.* **2012**, *51*, 2020−2067.
(9) You, J.; Dou, L.; Yoshimura, K.; Kato, T.; Ohya, K.; Moriarty, T.; Emery, K.; Chen, C.-C.; Gao, J.; Li, G.; Yang, Y. *Nat. Commun.* **2013**, *4*, 1446.
(10) Kazaoui, S.; Minami, N.; Tanabe, Y.; Byrne, H. J.; Eilmes, A.; Petelenz, P. *Phys. Rev. B* **1998**, *58*, 7689−7700.
(11) Schlenker, C. W.; Thompson, M. E. *Chem. Commun.* **2011**, *47*, 3702−3716.
(12) Peumans, P.; Uchida, S.; Forrest, S. R. *Nature* **2003**, *425*, 158−162.
(13) Peumans, P.; Yakimov, A.; Forrest, S. R. *J. Appl. Phys.* **2003**, *93*, 3693−3723.
(14) Lassiter, B. E.; Wei, G.; Wang, S.; Zimmerman, J. D.; Diev, V. V.; Thompson, M. E.; Forrest, S. R. *Appl. Phys. Lett.* **2011**, *98*, 243307−3.
(15) Wei, G.; Lunt, R. R.; Sun, K.; Wang, S.; Thompson, M. E.; Forrest, S. R. *Nano Lett.* **2010**, *10*, 3555−3559.
(16) Wei, G.; Xiao, X.; Wang, S.; Sun, K.; Bergemann, K. J.; Thompson, M. E.; Forrest, S. R. *ACS Nano* **2012**, *6*, 972−978.
(17) Zimmerman, J. D.; Xiao, X.; Renshaw, C. K.; Wang, S.; Diev, V. V.; Thompson, M. E.; Forrest, S. R. *Nano Lett.* **2012**, *12*, 4366−4371.
(18) Wei, G.; Wang, S.; Renshaw, K.; Thompson, M. E.; Forrest, S. R. *ACS Nano* **2010**, *4*, 1927−1934.
(19) Wei, G.; Xiao, X.; Wang, S.; Zimmerman, J. D.; Sun, K.; Diev, V. V.; Thompson, M. E.; Forrest, S. R. *Nano Lett.* **2011**, *11*, 4261−4264.
(20) Anthony, J. E. *Chem. Mater.* **2011**, *23*, 583−590.
(21) Sonar, P.; Lim, J. P. F.; Chan, K. L. *Energy Environ. Sci.* **2011**, *4*, 1558−1574.
(22) Hesse, H. C.; Weickert, J.; Hundschell, C.; Feng, X.; Muellen, K.; Nickel, B.; Mozer, A. J.; Schmidt-Mende, L. *Adv. Energy Mater.* **2011**, *1*, 861−869.
(23) Ford, W. E.; Kamat, P. V. *J. Phys. Chem.* **1987**, *91*, 6373−6380.
(24) Kircher, T.; Lohmannsroben, H. G. *Phys. Chem. Chem. Phys.* **1999**, *1*, 3987−3992.
(25) Baffreau, J.; Leroy-Lhez, S.; Van Anh, N.; Williams, R. M.; Hudhomme, P. *Chem.−Eur. J.* **2008**, *14*, 4974−4992.
(26) Baffreau, J.; Leroy-Lhez, S.; Hudhomme, P.; Groeneveld, M. M.; van Stokkum, I. H. M.; Williams, R. M. *J. Phys. Chem. A* **2006**, *110*, 13123−13125.
(27) Liu, Y.; Zhao, J. *Chem. Commun.* **2012**, *48*, 3751−3753.
(28) Schueppel, R.; Uhrich, C.; Pfeiffer, M.; Leo, K.; Brier, E.; Reinold, E.; Baeuerle, P. *ChemPhysChem* **2007**, *8*, 1497−1503.
(29) Uhrich, C.; Schueppel, R.; Petrich, A.; Pfeiffer, M.; Leo, K.; Brier, E.; Kilickiran, P.; Baeuerle, P. *Adv. Funct. Mater.* **2007**, *17*, 2991−2999.
(30) Wu, W.; Zhao, J.; Sun, J.; Guo, S. *J. Org. Chem.* **2012**, *77*, 5305−5312.
(31) Ziessel, R.; Allen, B. D.; Rewinska, D. B.; Harriman, A. *Chem.−Eur. J.* **2009**, *15*, 7382−7393.
(32) Vauthey, E. *ChemPhysChem* **2012**, *13*, 2001−2011.
(33) Yang, Y. F.; Arias, F.; Echegoyen, L.; Chibante, L. P. F.; Flanagan, S.; Robertson, A.; Wilson, L. J. *J. Am. Chem. Soc.* **1995**, *117*, 7801−7804.
(34) Veldman, D.; Meskers, S. C. J.; Janssen, R. A. J. *Adv. Funct. Mater.* **2009**, *19*, 1939−1948.
(35) Dastoor, P. C.; McNeill, C. R.; Frohne, H.; Foster, C. J.; Dean, B.; Fell, C. J.; Belcher, W. J.; Canipbell, W. M.; Officer, D. L.; Blake, I. M.; Thordarson, P.; Crossley, M. J.; Hush, N. S.; Reimers, J. R. *J. Phys. Chem. C* **2007**, *111*, 15415−15426.
(36) Kubo, Y.; Watanabe, K.; Nishiyabu, R.; Hata, R.; Murakami, A.; Shoda, T.; Ota, H. *Org. Lett.* **2011**, *13*, 4574−4577.
(37) Hanson, K.; Tamayo, A.; Diev, V. V.; Whited, M. T.; Djurovich, P. I.; Thompson, M. E. *Inorg. Chem.* **2010**, *49*, 6077−6084.
(38) Azenha, E. G.; Serra, A. C.; Pineiro, M.; Pereira, M. M.; de Melo, J. S.; Arnaut, L. G.; Formosinho, S. J.; Gonsalves, A. *Chem. Phys.* **2002**, *280*, 177−190.
(39) Pineiro, M.; Carvalho, A. L.; Pereira, M. M.; Gonsalves, A.; Arnaut, L. G.; Formosinho, S. J. *Chem.−Eur. J.* **1998**, *4*, 2299−2307.
(40) Sazanovich, I. V.; Kirmaier, C.; Hindin, E.; Yu, L. H.; Bocian, D. F.; Lindsey, J. S.; Holten, D. *J. Am. Chem. Soc.* **2004**, *126*, 2664−2665.
(41) Ulrich, G.; Ziessel, R.; Harriman, A. *Angew. Chem., Int. Ed.* **2008**, *47*, 1184−1201.
(42) Yu, L. H.; Muthukumaran, K.; Sazanovich, I. V.; Kirmaier, C.; Hindin, E.; Diers, J. R.; Boyle, P. D.; Bocian, D. F.; Holten, D.; Lindsey, J. S. *Inorg. Chem.* **2003**, *42*, 6629−6647.
(43) Rio, Y.; Sanchez-Garcia, D.; Seitz, W.; Torres, T.; Sessler, J. L.; Guldi, D. M. *Chem.−Eur. J.* **2009**, *15*, 3956−3959.
(44) Dorset, D. L.; McCourt, M. P. *Acta Crystallogr., Sect. A* **1994**, *50*, 344−351.
(45) Vandenheuvel, D. J.; Chan, I. Y.; Groenen, E. J. J.; Schmidt, J.; Meijer, G. *Chem. Phys. Lett.* **1994**, *231*, 111−118.
(46) Capozzi, V.; Celentano, G.; Perna, G.; Lorusso, G. F.; Minafra, A. *J. Lumin.* **2000**, *86*, 129−135.
(47) Ichida, M.; Sakai, M.; Yajima, T.; Nakamura, A. *Prog. Cryst. Growth Charact. Mater.* **1996**, *33*, 125−128.
(48) Li, J.; Komiya, S.; Tamura, T.; Nagasaki, C.; Kihara, J.; Kishio, K.; Kitazawa, K. *Physica C* **1992**, *195*, 205−208.
(49) Bartynski, A. N.; Trinh, C.; Panda, A.; Bergemann, K.; Lassiter, B. E.; Zimmerman, J. D.; Forrest, S. R.; Thompson, M. E. *Nano Lett.* **2013**, *13*, 3315−3320.
(50) Wang, S.; Mayo, E. I.; Perez, M. D.; Griffe, L.; Wei, G.; Djurovich, P. I.; Forrest, S. R.; Thompson, M. E. *Appl. Phys. Lett.* **2009**, *94*, 233304.
(51) Laha, J. K.; Dhanalekshmi, S.; Taniguchi, M.; Ambroise, A.; Lindsey, J. S. *Org. Process Res. Dev.* **2003**, *7*, 799−812.